Bayesian uncertainty analysis of inversion models applied to the inference of thermal properties of walls

Séverine Demeyer, V. Le Sant, A. Koenen, N. Fischer, Julien Waeytens, Rémi Bouchié

▶ **To cite this version:**

Séverine Demeyer, V. Le Sant, A. Koenen, N. Fischer, Julien Waeytens, et al.. Bayesian uncertainty analysis of inversion models applied to the inference of thermal properties of walls. Energy and Buildings, 2021, 249, pp.111188. 10.1016/j.enbuild.2021.111188 . hal-04353797

HAL Id: hal-04353797
https://hal.science/hal-04353797v1

Submitted on 19 Dec 2023

HAL is a multi-disciplinary open access archive for the deposit and dissemination of scientific research documents, whether they are published or not. The documents may come from teaching and research institutions in France or abroad, or from public or private research centers.

L'archive ouverte pluridisciplinaire **HAL**, est destinée au dépôt et à la diffusion de documents scientifiques de niveau recherche, publiés ou non, émanant des établissements d'enseignement et de recherche français ou étrangers, des laboratoires publics ou privés.

Bayesian uncertainty analysis of inversion models applied to the inference of thermal properties of walls

Séverine Demeyer*, **V. Le Sant, A. Koenen and N. Fischer**
Laboratoire National de Métrologie et d'Essais, 29 avenue Roger Hennequin, 78197 Trappes Cedex
*E-mail: severine.demeyer@lne.fr

Julien Waeytens
Univ. Gustave Eiffel, IFSTTAR,
14-20 boulevard Newton, 77447, Marne la Vallée Cedex 2, France
E-mail: julien.waeytens@univ-eiffel.fr

Rémi Bouchié
Centre Scientifique et Technique du Bâtiment,
84 avenue Jean Jaurès, Champs-sur-Marne, 77447 Marne-la-Vallée, France
E-mail: remi.bouchie@cstb.fr

Abstract.

In this work, we propose a fully Bayesian uncertainty analysis of the indirect measurement of thermal properties of walls from in-situ temperature and flux measurements, obtained with an active method, using a one dimensional transient thermal model. We show that this approach is able to take into account the uncertainty of the inputs of the thermal model and the uncertainty of the output observations, for a more reliable uncertainty estimation of the *calibration parameters* and any derived quantity. For this problem, we improve the classical Bayesian inversion model by taking into account underestimated uncertainty on reported output observations, which is a frequently encountered issue in practice. We provide some recommendations for a wider applicability of the method. We illustrate the principles of uncertainty evaluation of the *Guide to the Expression of Uncertainty in Measurement* [BIPM et al., 2008a] in terms of a real case study to evaluate the thermal resistance of a multilayer wall placed in a climatic chamber. For this application, we compare results of the Bayesian inversion with classical steady-state results in comparable experimental conditions. We perform a sensitivity analysis to study the effect of duration and input uncertainties and we make recommendations. R code is made available that enables a Bayesian uncertainty evaluation of inversion models for related applications.

1. Introduction

In the context of building energy management or retrofit interventions, thermal resistance of walls is used in standard heat transfer models as a parameter for building performance simulations [Iglesias et al., 2018]. Due to the cost of wall thermal characterization, tabulated values for thermal properties are typically used as inputs of the energy models [Iglesias et al., 2018].

The in-situ measurement of the thermal resistance of walls should, for instance, contribute to decrease the gap between actual and predicted consumption to have more reliable energy-savings strategies or to have a more reliable assessment of the effectiveness of retrofit interventions [Simon et al., 2018].

The present study is part of the French National Research project named RESBATI whose main objective is to develop a portable measurement device for evaluating the thermal resistance of opaque building walls on site. The result of the thermal resistance measurement should be provided with its uncertainty [Ha et al., 2020]. The active method (a thermal gradient inside the wall is created by a step heating excitation applied on a face) chosen in the project allows to estimate the thermal resistance of a building wall in all seasons, for any type of building and use (occupied or otherwise) in quite a short measurement time (less than three days) which improves on classical steady-state or dynamic methods [François et al., 2020], [Ha et al., 2020]. In this paper, we consider that the thermal resistance of a wall is measured indirectly from in-situ temperature and flux measurements. This is an inverse problem classically encountered in building physics [Rouchier, 2018].

To carry out the identification method, a direct model (here a thermal model) is embedded in a simulator $\eta(X, \theta)$ whose inputs are the calibration parameters θ (called *primary unknowns* in [Kaipio and Fox, 2011]), and the experimental conditions X, see Figure 1. In practice, [Kaipio and Fox, 2011] mention that it is very seldom that the primary unknowns θ are the only *input unknowns*. The vector X gathers all the uncertainty sources, called here *input parameters*, having an effect on the measurement result of the thermal resistance and that can be modeled by a probability distribution. In the following, the uppercase notation X denotes a random vector, whereas the lowercase x denotes a particular observed value of X. In this paper, we have chosen a one-dimensional transient thermal model as a good approximation of the physical phenomenon with a low computational cost. Since the thermal model does not take into account lateral flux in the building wall, the user has to make sure that the flux is close to 1D, which makes the simulator fit for purpose.

The identification process, illustrated in Figure 1, also called calibration or inversion, consists to find the values $\hat{\theta}$ of the input calibration parameters of the thermal model so that the output $\eta(x, \hat{\theta})$ is as closed as possible to the experimental values $y(x)$ obtained in the experimental conditions x. The classical techniques for solving the minimization problem pertaining to inversion are based on least squares methods (e.g. Levenberg-Marquardt algorihm), maximum-likelihood (ML) and

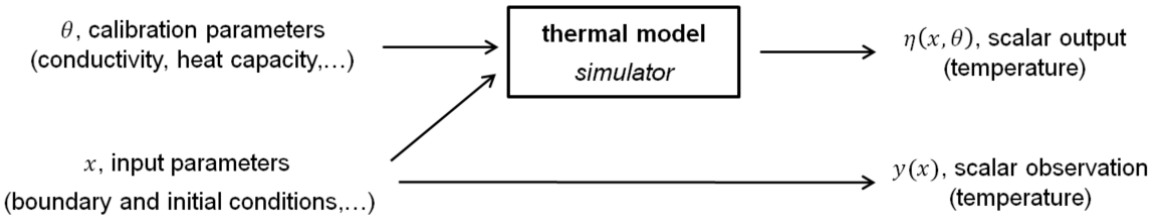

Figure 1. Schema of a calibration (inversion) procedure.

Bayesian analysis. A description and a comparison of these inversion techniques can be found in [Rouchier, 2018] and [Kaipio and Fox, 2011]. In Bayesian statistics, the inverse problem is regularized statistically through the modeling of prior distribution [Kaipio and Fox, 2011]. Prior distributions represent prior degrees of belief on the (usually) unique but unknown values of the inputs which are turned into posterior degrees of belief (posterior distributions) via the Bayes formula when observations are available. The reader interested in generalities about Bayesian statistics can refer to [Gelman et al., 2013] and [Box and Tiao, 1992].

Bayesian inversion requires advanced computational tools like Markov Chain Monte Carlo methods (MCMC) to sample from the posterior distributions [Metropolis et al., 1953], [Chib and Greenberg, 1995], [Robert and Casella, 2013]. For a tutorial on the class of MCMC algorithms classically used for Bayesian inversion (the Metropolis-Hastings algorithm) the reader is referred to [Klauenberg and Elster, 2016]. Recently, Bayesian calibration using in-situ measurements has been widely used for the inference of thermal properties and their associated uncertainties. To cite a few, [Berger et al., 2016] tackled the estimation the thermal conductivity and the internal convective heat transfer coefficient of a wall with 3 layers from one year experimental data, [Iglesias et al., 2018] addressed the estimation of the thermal resistance and the heat capacity of unit area of a homogeneous wall based on 7 days of measurements, [Thébault and Bouchié, 2018] considered the estimation of the HLC with the ISABELE method, [Simon et al., 2018] tackled the estimation of the thermal conductivity and the heat capacity of the wall based on 8 days measurement campaign, [Rodler et al., 2019] addressed the estimation of the thermal conductivity and the volumetric heat capacity from a few days measurements.

This paper focuses on uncertainty propagation in inversion models. A widespread approach is to consider input uncertainty sources as negligible or small enough to be aggregated with uncertainties on the outputs [Perrin and Durantin, 2019]. Such an approach is followed e.g. in [Simon et al., 2018] and [Berger et al., 2016]. However, if the input uncertainties are not negligible or even if there is no information about these input uncertainties, ignoring these uncertainties may result in biased estimated calibration parameters [Perrin and Durantin, 2019]. The difficulty that arises for uncertainty propagation is that there is usually no close functional form to describe the relation between the uncertainty sources and the estimate of the calibration

parameters [Wang and Zabaras, 2004]. Many approaches have been developped to create approximate relationships through which uncertainties are propagated. An example of uncertainty propagation using the variance-covariance matrix of estimated parameters with the ordinary least squares (OLS) method and a (thermal) model reduction can be found in [François et al., 2020]. The analytical expression of the outputs in function of the initial and the boundary conditions, e.g. using discretized heat transfer equations as in [Iglesias et al., 2018] provides the "missing" relationship between the uncertainty sources and the estimates of the calibration parameters (obtained as Bayesian estimates of non linear regression parameters in [Iglesias et al., 2018]). [Thébault and Bouchié, 2018] and [Gori and Elwell, 2018] establish posterior relationships between the estimated parameters taken as the maximum at posteriori (MAP) and the uncertain inputs (e.g. posterior profile at MAP). Although the Bayesian approach conceptually allows to take into account measurement uncertainty in both inputs and outputs, [Perrin and Durantin, 2019] point out that little work has been done to uncertainties on inputs. The recent work by [Rodler et al., 2019] combines Metropolis-Hastings with Monte Carlo sampling from the uncertainty sources in an attempt of full Bayesian inversion.

The goal of the paper is to provide guidance on input uncertainty propagation in Bayesian inversion for the in-situ estimation of thermal parameters from temperature and flux measurements using a 1D thermal model. In this paper, we assume that the steps of review of the uncertainty sources, selection of the most influential and finally the prior quantification and modeling of uncertainty attached to all of them has been done before performing the Bayesian uncertainty analysis of the inversion problem. We show that uncertainty propagation of the experimental conditions through the inversion model can be performed by a fully Bayesian analysis of the inversion problem by posterior sampling from the joint prior distribution of the calibration parameters and the uncertain experimental conditions, following an approach similar to [Demeyer et al., 2021] and [Higdon et al., 2004]. The results are calculated with Markov Chain Monte Carlo methods (MCMC) and an introduction to these methods is given.

Among the various simulation studies [Ha et al., 2020] and experimental works carried out within the RESBATI project, the use case of this paper focuses on the thermal measurements obtained on a IWI (Inner Wall Insulation) test wall built within the project and circulated between LNE and CSTB. Here, we compare results from the Bayesian analysis of the thermal measurements obtained in an energy room at LNE with the results from the steady-state guarded hot box method at CSTB and we perform a sensitivity analysis to study the effect of measurement duration and the level of uncertainty.

2. Bayesian calibration under uncertainty

2.1. General formulation

Denoting $y = (y_1, ..., y_N)$ the vector of output measurements, $X = (X_1, ..., X_N)$ where $X_i = (X_{i1}, ..., X_{id})^T$, the $N \times d$ matrix of uncertain input variables and θ the vector of calibration parameters, the fully Bayesian inversion model writes

$$y = \eta(X, \theta) + \varepsilon \tag{1}$$

$$X \sim \pi(X) \tag{2}$$

$$\theta \sim \pi(\theta) \tag{3}$$

where $\eta(X, \theta) = (\eta(X_1, \theta), ...\eta(X_N, \theta))$ denotes the vector of simulation outputs, $\varepsilon = (\varepsilon_1, ..., \varepsilon_N)$ denotes the vector of output measurement error, $\pi(X)$ and $\pi(\theta)$ denote respectively the prior distributions of X and θ.

The unknown vector X is classically represented with an error in variable model (see [Perrin and Durantin, 2019]) as a deviation from a known central value x (see discussion section 2.5)

$$X = x + \zeta \tag{4}$$

where $\zeta = (\zeta_1, ..., \zeta_N)$ denotes the matrix of input measurement error and $x = (x_1, ..., x_N)$ denotes the matrix of input observations.

The random variables ε_i and ζ_i, for $i = 1, ..., N$, are commonly modeled as centered Gaussian variables with known covariance matrix denoted Σ_ε and Σ_ζ respectively [Perrin and Durantin, 2019]. Furthermore θ, ε and ζ are assumed statistically independent.

2.2. Modeling excess variance

Model (1) assumes that output observations are equivalent to the calibrated simulations, their difference being explained by the reported measurement uncertainties. In practice, an excess variability of the y_i with respect to (w.r.t.) the variability explained by the measurement uncertainty may be observed. Under the assumption that the simulator is fit for purpose, not taking into account excess variance may lead to biased estimates of the calibration parameters.

Under the hypothesis that the excess variability is due to a missing term in the uncertainty budget ‡, we propose to model the excess variability (also called heterogeneity of data) with an adjustment factor $\sigma > 0$ as in [Bodnar and Elster, 2014] and [Mana et al., 2012]

$$y = \eta(X, \theta) + \sigma\varepsilon \tag{5}$$

‡ In this paper, we assume that the excess variability of the time-varying thermal measurements y_i where i indexes time, comes from a missing influential source of uncertainty or from varying, not controllable, conditions during the recording period (noise).

The parameter σ is related to the Birge ratio, that is often used in metrology to enlarge quoted uncertainties when combining inconsistent measurement results on the same measurand [Bodnar and Elster, 2014]. As shown in [Mana et al., 2012], the Birge ratio can be interpreted as the most probable value of such an adjustment factor.

According to [Bodnar and Elster, 2014], it can be assumed that σ^2 follows a priori an inverse chi-squared distribution $\sigma^2 \sim \text{InvChi}^2(\nu_0, s_0^2)$, in which case the marginal distribution of observations w.r.t σ^2 is multivariate t-distributed

$$y \sim t_{\nu_0}\left(\eta(X,\theta), s_0^2\Sigma_\varepsilon\right) \tag{6}$$

A poorly informative prior for σ^2, centered on 1, can be obtained with $\nu_0 = 2$ and $s_0^2 = 2$.

Remarks

- The prior degree of freedom ν_0 can be viewed as allowing "uncertainty on the uncertainty" contained in Σ_ε which comes to considering reported uncertainties as point estimates of the unknown standard deviations.§ The assumption that the missing source of uncertainty is common to all measurements translates into ν_0 being common to all measurements.
- Additive random effects ‖ could be used to model excess variance if measurement results y_i were obtained from uncertainty analyses performed independently, for instance by various teams or with different measurement devices. They have become common practice for instance when building consensus estimates in meta-analysis and interlaboratory comparisons [Bodnar et al., 2017]. For such applications, individual degrees of freedom ν_i are taken into account when they are available, see [Toman and Possolo, 2009].

2.3. Bayesian inference

In order to perform a full Bayesian analysis of the inversion problem, calibration parameters θ are augmented with the latent variables X and the heterogeneity variance parameter σ^2. The Bayes formula provides the joint posterior distribution for (θ, X, σ^2)

$$\pi(\theta, X, \sigma^2|y) \propto l(y|\eta(X,\theta), \sigma^2)\pi(\theta)\pi(\sigma^2)\pi(X) \tag{8}$$

§ For instance, the GUM uses the so-called Welch-Satterthwaite formula to estimate the degrees of liberty associated with a measurement result assuming it is t-distributed.

‖ The conventional random effects model considers the following model for the output observations

$$y = \eta(X,\theta) + \lambda + \varepsilon \tag{7}$$

where $\lambda = (\lambda_1, ..., \lambda_N)$ gathers for instance the team effects under the assumptions that $\lambda_i \sim_{iid} N(0, \sigma^2)$, $\varepsilon_i \sim N(0, u_i^2)$ and that the λ_i and the ε_i are independent.

where $l(y|\eta(X,\theta),\sigma^2)$ is the likelihood, $\pi(\theta)$, $\pi(\sigma^2)$, $\pi(X)$ are the prior distributions of θ, σ^2 and X respectively, assumed independent. The prior distribution $\pi(\theta)$ is usually based on expert knowledge or tabulated values. The prior distribution for σ^2 can be chosen as poorly informative when the dataset is large. In order to account for the input uncertainty sources X, $\pi(X)$ is a data-driven prior distribution based on (4).

In this paper, the quantity of interest is the joint posterior distribution $\pi(\theta, X|y)$ obtained by integrating the joint posterior distribution out σ^2

$$\pi(\theta, X|y) = \int_0^{+\infty} \pi(\theta, X, \sigma^2|y) \mathrm{d}\sigma^2 \tag{9}$$

For a well-chosen prior distribution $\pi(\sigma^2)$, a closed form expression can be computed for (9). For instance, using $\sigma^2 \sim \mathrm{Inv}-\mathrm{chi2}(\nu_0, s_0^2)$ yields

$$\pi(\theta, X|y) \propto \pi(\theta)\pi(X) l_{int}(y|X,\theta) \tag{10}$$

where $l_{int}(y|X,\theta) = t_{\nu_0}\left(\eta(X,\theta), s_0^2\Sigma_\varepsilon\right)$

2.4. Posterior simulation with Markov Chain Monte Carlo algorithms

Integrals (8), (9) or (10) are usually intractable and require simulation methods like Markov Chain Monte Carlo (MCMC) methods. MCMC methods provide a flexible and powerful tool for sampling from an arbitrary distribution. These methods construct a sequence of dependent values which form a Markov chain with stationary distribution equal to the sought posterior distribution. The Metropolis-Hastings (MH) algorithm [Metropolis et al., 1953], [Chib and Greenberg, 1995] constitutes a popular class of MCMC methods. The interesting feature of the MH algorithm is that it only requires to know the posterior distribution up to a proportionality constant, i.e. the right-hand part of Eq.8 or Eq.10, which makes it particularly suited for calibration problems. The MH algorithm can be used in conjunction with the Gibbs algorithm if conditional posterior distributions are tractable for a subset of parameters (the so-called *Metropolis-within-Gibbs* algorithm). The sequence of values is considered after a burn-in period and often the chains are thinned (i.e. only each 10th value is used) to decrease the autocorrelation of the chains.

The Metropolis Hastings algorithm for sampling from the posterior distribution of (θ, X) given y in (10) is given in algorithm (1). The *initialization* step (line 1) provides a starting point for the iterative algorithm which can be sampled from the prior distributions or near a best physical point if available or obtained from computational techniques based e.g. on the gradient (Lagrange,...). At each iteration l, a (multidimensional) *candidate* $(\theta^{(c)}, X^{(c)})$ is sampled (line 5) and the corresponding output of the thermal simulation $\eta(\theta^{(c)}, X^{(c)})$ is computed (line 6). The *acceptance/rejection* step lines 8, 9 and 10 is based on the ratio of posterior distributions

(known up to the same constant, that disappears in the ratio)

$$\alpha = \frac{\pi(\theta^{(c)}, X^{(c)}|y)}{\pi(\theta^{(l-1)}, X^{(l-1)}|y)} \tag{11}$$

A candidate point with ratio $\alpha < 1$ has probability α to be selected which corresponds to $P(u < \alpha)$ where $u \sim Unif(0,1)$. If a candidate is accepted, the candidate is the new point of the chain, otherwise the previous point is added to the chain. It is important to note that at each iteration an element is added to the chain, being either the candidate or the previous point. For computational reasons, the log-posteriors are used (line 2 for the log-posterior of the starting point and line 7 for the log-posterior of the candidate point).

Algorithm 1 Metropolis-Hastings algorithm for Bayesian calibration under uncertainty

Input: measurements x_i, y_i, t_i ;

Output: M samples from the posterior distribution $\pi(\theta, X|y)$ according to (10);

1: initialize: $\left(\theta^{(1)}, X^{(1)}, \eta^{(1)} = \eta(X^{(1)}, \theta^{(1)})\right)$;
2: compute $a = \ln(\pi(\theta^{(1)}, X^{(1)}|y))$;
3: **repeat**
4: $\quad l \leftarrow l + 1$;
5: $\quad$ sample $\theta^{(c)} \sim N_d(\theta^{(l-1)}, \Sigma_\theta^{(l-1)})$ and $X^{(c)} \sim N_N\left(X^{(l-1)}, \Sigma_X^{(l-1)}\right)$;
6: $\quad$ generate $\eta^{(c)} = \eta(X^{(c)}, \theta^{(c)})$;
7: $\quad$ compute $b = \ln(\pi(\theta^{(c)}, X^{(c)}|\eta^{(c)}))$;
8: $\quad$ let $\alpha = \min\left(\exp(b-a), 1\right)$ and $u \sim \mathrm{Unif}(0,1)$;
9: $\quad$ if $\alpha \geq u$ then $\theta^{(l)} = \theta^{(c)}$ and $X^{(l)} = X^{(c)}$;
10: $\quad$ else $\theta^{(l)} = \theta^{(l-1)}$ and $X^{(l)} = X^{(l-1)}$;
11: $\quad a \leftarrow b$
12: **until** $l = M$

2.5. Discussion

The Bayesian approach allows a flexible modelling of the prior distributions $\pi(X)$ and $\pi(\theta)$ due to the use of MCMC simulation methods, among which the Gaussian, Student, rectangular, triangular and trapezoïdal distributions that are commonly used to represent uncertainty on input quantities e.g. in metrology (see GUM-S1 [BIPM et al., 2008b]). For instance, the Gaussian distribution can be used to model inputs resulting from an uncertainty propagation (e.g. following the GUM propagation of variance [BIPM et al., 2008a]) like the solar aperture and the volumetric flowrate. Generally, the prior on θ consists in a rectangular distribution defining bounds inside which the unknown value is supposed to lie, to improve the computational efficiency of the inversion method. For example, the bounds associated with thermophysical properties of material can usually be found in literature

[Heo et al., 2012], [ASHRAE, 2017]. More generally, guidelines for assessing the uncertainty of inputs used in building energy models can be found in [Macdonald, 2002] and [Heo et al., 2012].

To account for complex uncertain inputs like those related to time (e.g. occupancy, weather, usage...), a discrepancy term $\delta(x)$, function of these inputs, is usually added to (1) [Heo et al., 2012] and $\pi(X)$ is modeled as a Gaussian Process [Rasmussen and Williams, 2006], [Santner and Notz, 2003]. A complete Bayesian framework for modelling an additional discrepancy term in inversion is proposed in [Higdon et al., 2004], [Kennedy and O'Hagan, 2001]. In this paper, due to the active method, temperature and flux measurements are likely to be non-stationary time processes that would require modeling using e.g. Gaussian processes functions of both x and y. For simplicity, we choose to model the uncertain time varying inputs and outputs following (4) and (1) respectively and to leave the thorough modeling of input and output time series and their associated uncertainties in Bayesian inversion as a perspective of this work. Indeed, for the analysis of the real case study, such further work did not prove necessary.

In this paper, we propose a fully Bayesian approach of inversion problems to propagate uncertainties of input parameters during the inversion procedure, which comes to treat all parameters as *calibration parameters* in classical Bayesian inversion. Such an approach is even recommended as a baseline of any Bayesian inversion procedure in [Higdon et al., 2004]. Indeed, according to [Higdon et al., 2004], even if we believe that the true physical value is known, allowing a slight deviation from the true physical value (similar to representation (4)) may produce an empirically better model of the reality. Furthermore, estimations of the calibration parameters may not even be interpreted as estimates of the true physical values of these parameters [Higdon et al., 2004]. Rather, they are by nature a 'best fit' estimate of θ depending on the many hypotheses (among which that the thermal model is a perfect fit of the physical phenomenon) and the experimental conditions involved in the whole process.

In this paper, the use of an active method on a short period (24 hours) allows to limit bias due to the sensitivity of the inversion procedure to the environmental conditions. Indeed, the effect of occupancy, weather and usage are potentially the most influential on the measure of thermal parameters (or more generally the energy performance) but also the most uncertain [Goffart et al., 2017]. If any, model approximation (assumed small) is taken into account in the free variance parameter σ^2 used to capture the excess variance with respect to the reported uncertainties, with the aim of limiting bias of the estimated calibration parameters due to modeling.

3. Application to the in-situ estimation of the thermal resistance of a wall

3.1. Motivation and context

The thermal resistance R ($\mathrm{m^2\,K\,W^{-1}}$) of the enveloppe of a building is an indicator of the thermal performance of the building. Within the RESBATI project, a measurement method of the thermal resistance of opaque walls has been developed to produce in-situ results with an associated uncertainty in less than three days.

In order to evaluate the performance of the method, a test wall of dimensions 2 meters by 2 meters with inner wall insulation (IWI) was built. The insulation layer is made of EPS (expanded polystyrene). In this application, we compare the results obtained by the active method on the test wall placed in an energy room at LNE, France (see sections 3.2 and 3.5.3), with results obtained with the steady-state guarded hot box method [ISO 8990:1994, 1994] at CSTB, France (see section 3.5.2). For this application, the steady-state guarded hot plate method [ISO 8302:1991, 1991] (see section 3.5.1) is used to estimate the thermal resistance of the insulation layer (EPS). The description of the experimental conditions of each method is given.

3.2. Description of the energy room REBECCA at LNE

The energy room at LNE is a climatic chamber inside another climatic chamber. It is composed of an internal cell with the dimensions of a dwelling (3.42 m of side on 2.29 m high, surface of the test specimen 7.83 $\mathrm{m^2}$). The latter is surrounded by 4 climatic chambers in which it is possible to modify the temperature between $-7\,^{\circ}\mathrm{C}$ and $35\,^{\circ}\mathrm{C}$ and to generate any type of transient regime (hot cold, cycle, etc.). The four surrounding boxes (front cell, guard, floor and ceiling) can be controlled separately (Figure 2). The REBECCA (Research and Testing of Buildings and Heat Emitters under Artificial Climate) cell is built to reproduce the principle of a guarded hot box test but with more room inside to install additional devices. The front panel is equipped with the specimen to be studied. In order to ensure that the entire heat flow passes through the test specimen, the 5 walls of the inner cell in contact with the thermal guard are insulated with Vacuum Insulated Panels having a thermal resistance greater than $10\,\mathrm{m^2\,K\,W^{-1}}$. The test can be carried out under steady state condition, which occurs after a long period of time, or in a transient way like temperature ramp.

3.3. Description of the measurement process with the active method

The test wall is installed in the REBECCA cell and an active method is used to produce faster in-situ results using a heating module, temperature and flux sensors placed on the wall, as displayed in Figure 3.

The active method uses a prototype built by the laboratory CERTES (Centre d'Études et de Recherche en Thermique, Environnement et Systèmes, Université Paris Est Créteil, France) within the RESBATI project. The prototype is a cube of 60 cm of side. One side is open; in the opposite side 24 DC halogen spots of 20 W are

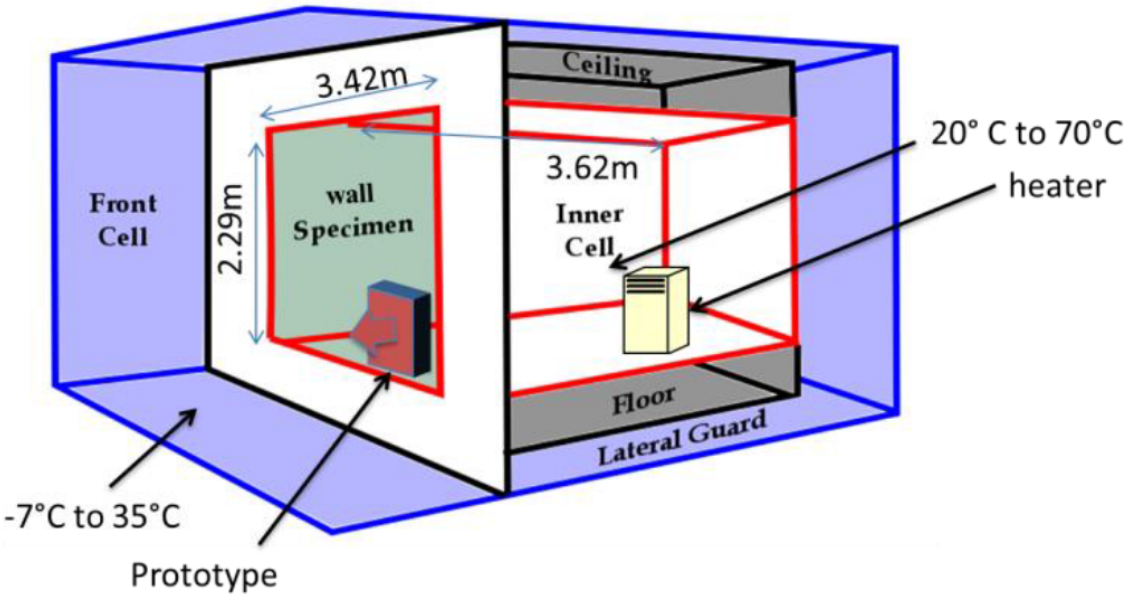

Figure 2. Schematic diagram of the energy room called 'REBECCA' at LNE, France, from [Koenen et al., 2019].

positioned. The maximum electrical power is 480 W that can be adjusted depending on the test scenario. The four remained faces are insulated with reflective material with a low emissivity. In the front side in contact with the IWI, a heat flow meter with thermocouples is positioned. The IWI is then heated by the halogen spots. The heat flow that goes in the wall through the heat flow sensor and the surface temperatures of the wall are measured every 2 s. A step heating excitation which can reach several days is used for all experiments. A schematic description and a view of the experimental set-up are presented in Figure 3 and Figure 4. A number of 30 thermocouples are positioned along the heat flow meter to validate the one dimension hypothesis.

The heat flow sensors were calibrated in the LNE guarded hot plate at different mean temperatures T (mean of external and internal temperatures) and temperature difference ΔT between the internal and external temperatures. All thermocouples were calibrated at LNE. A test lasts 24 h after steady state condition is achieved. This can continue several days depending on the thermal properties of the walls.

The RESBATI device induces a constant power of 105 W. The external cell was cooled at 0 °C and the internal room was heated at 20 °C in order to obtain a temperature difference ΔT of 20 °C between the two sides of the wall. The heat flow going through the wall in the RESBATI area is measured continuously and reaches around 10 W m^{-2} after 10 h and remains constant afterwards.

In this application, the standard uncertainty (evaluated at LNE) associated with the inner and outer surface temperatures (Tsi and Tse respectively) is $u(Tsi) = u(Tse) =$ 0.5 °C and the standard uncertainty associated with the absorbed flux q_{int} is $u(q_{int}) =$

329 $3\%q_{int}$ W m^{-2}.

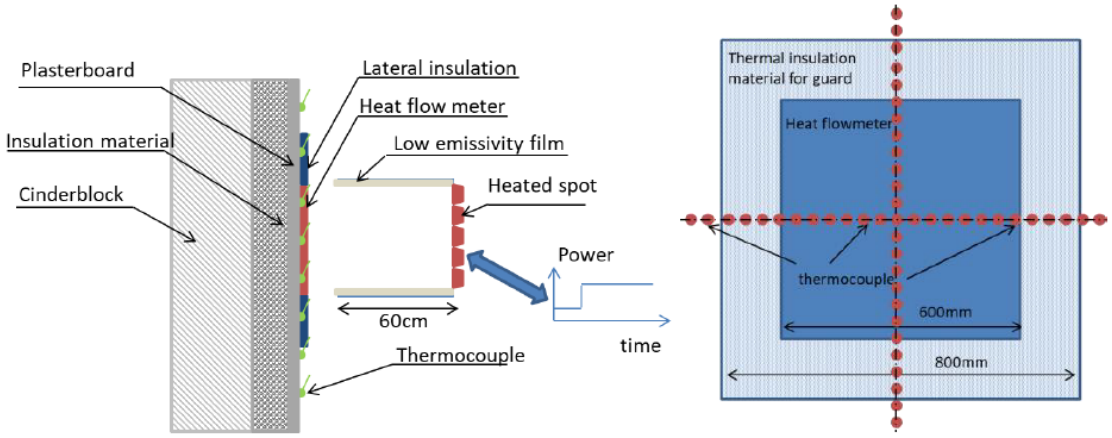

Figure 3. Schematic view of the experimental setup (side view, face view), from [Koenen et al., 2019].

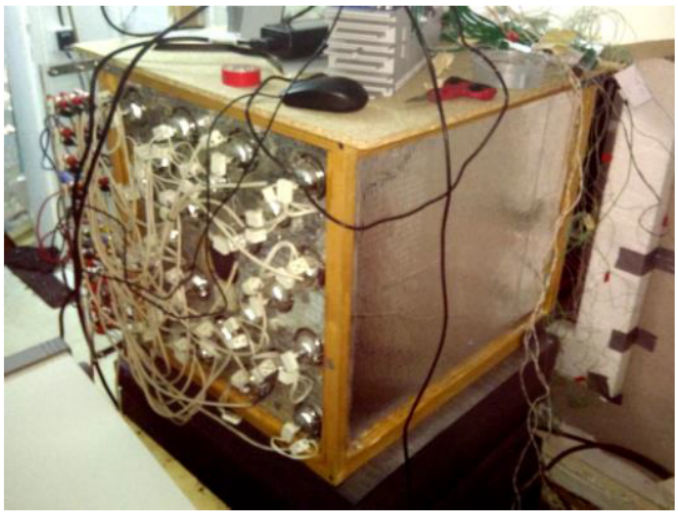

Figure 4. View of the active method prototype, from [Koenen et al., 2019].

330 The thermal resistance of a multi-layer wall is measured indirectly from temperature
331 and flux measurements after the identification of the parameters θ of a thermal model
332 $\eta(X, \theta)$ (here with $X = (Tse, q_{int})$, see section 3.4) using the Bayesian approach
333 described section 2. A 1D transient thermal model solved with a finite element
334 method in space and a Euler implicit time integration scheme was chosen in this
335 study that takes the heat capacity of unit area cw_i (J m^{-2} K^{-1}) and the thermal
336 conductivity k_i (W m^{-1} K^{-1}) of each layer i as calibration inputs gathered in the vector
337 $\theta = \{cw_i, k_i\}_{i=1,\dots,I}$ where $I = 4$ is the number of layers.

The thermal resistance of the wall is expressed as the sum of the thermal resistance

R_i of each layer

$$R = \sum_{i=1}^{I} R_i, \text{with } R_i = \frac{l_i}{k_i} \tag{12}$$

where l_i (m) is the thickness of layer i (in this study, l_i is considered known, see values in Table 7). The estimate of the thermal resistance and its associated uncertainty are obtained with the Monte Carlo method applied to (12) using the samples from the posterior distributions of the k_i. In particular, R_2 denotes the thermal resistance of the insulation layer.

Comments on the identifiability of the thermal parameters With this choice of thermal model and the low number of used sensors, we numerically observe that only the joint distribution of the input thermal parameters is identifiable but not its individual constituents (various combinations of values for cw_i and k_i could produce close thermal resistance values). This is a common situation in inversion problems, see the point of [Higdon et al., 2004] discussed in section 2.5, which is overcome here by considering that the thermal resistance (here, the quantity of interest) is identifiable but *a priori* not the cw_i and k_i taken individually. It is thus important to take samples from the joint posterior distribution to perform the Monte Carlo estimation of the thermal resistance.

Still, from virtual testing and model-based sensitivity analysis, the thermal conductivity of the insulation layer k_2 should be identifiable for this application. Thus, the comparison of the posterior distribution of k_2 with an experimental result (e.g. obtained with GHP) could be used as an indication of the ability of the method to estimate the thermal resistance of the insulation layer (calculated as $R_2 = l_2/k_2$), see section 3.5.3. Besides, in this study, the thickness of the layers of the wall is assumed to be known, but in general the thickness should be estimated as well with prior knowledge e.g. based on approximate measurements or from the design of the wall. More generally, identifiability issues are tackled with the use of informative prior distributions.

3.4. Review of uncertainty sources to specify X

In order to perform a sound uncertainty analysis, the first step is to deeply analyse the measurement process by performing the most exhaustive review of the uncertainty sources pertaining to it (even those that are not quantifiable). This is a demanding brainstorming step involving both experts of the field and statisticians. The classical tool for such a task is the Ishikawa diagram, which is used in the GUM [BIPM et al., 2008a] to review the sources of uncertainty involved in a measurement process.

Figure 5 displays an instance of an Ishikawa diagram pertaining to the measurement process of the thermal resistance of a wall using the RESBATI prototype. Uncertainty sources are divided into five categories shortly described thereafter.

Means: refers to all the uncertainty sources involved with the measurements (sensors, reference materials, standards), here limited to sensors;

Method: refers to all uncertainty sources related to the measurement procedure and the data analysis which consists here in an identification method;

Wall/Enveloppe: refers to the object of the measurement, here the wall; for this application, the thermo-physical properties are the calibration parameters of the thermal model (see Figure 1);

Environment: refers to the variations of the experimental conditions during the process, here in the energy room;

Operator: refers to the uncertainty arising from the interpretation and the implementation of the procedure by operators involved in the whole process.

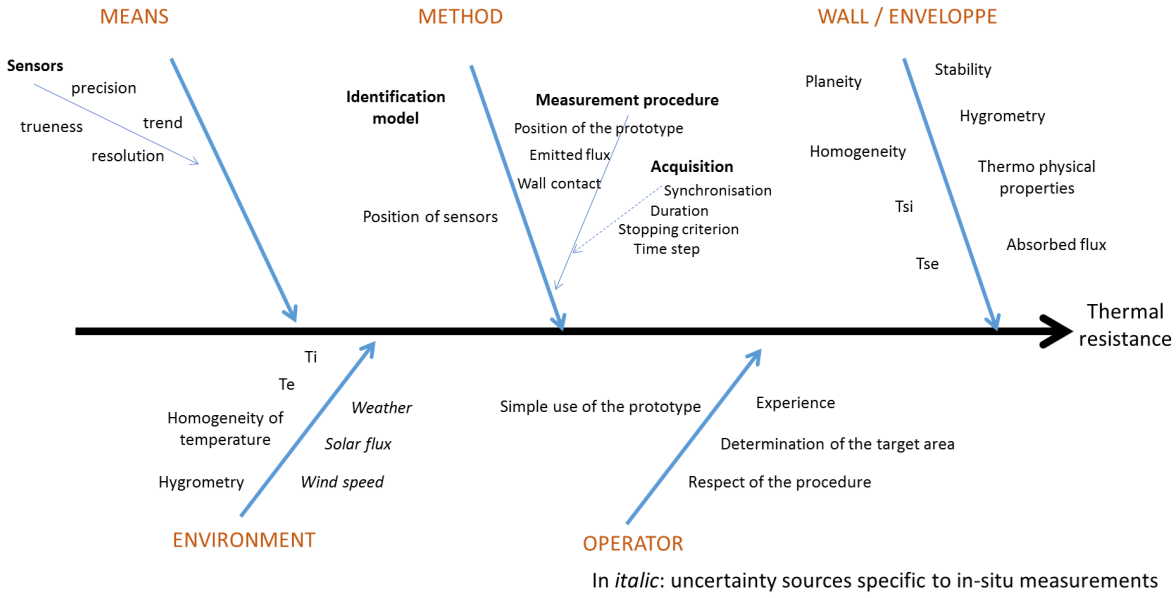

Figure 5. Ishikawa diagram for the thermal resistance.

Figure 6 describes the uncertainty sources pertaining to the identification model i.e to the thermal model and the inversion procedure.

In practice, only the most influential quantifiable uncertainty sources X are kept for the uncertainty analysis. Such a selection can be performed with sensitivity analysis methods [Saltelli et al., 2004] and/or by experts based on prior knowledge or information. It is important to note that the combined effect of unquantifiable uncertainty sources, assumed to vary randomly when repeating measurements, can be taken into account when processing measurements.

Here, we choose to focus only on $X = (Tse, q_{int})$ as an example of uncertainty propagation associated with temporal measurements.

3.5. Results for IWI test wall

In this section, we compare the estimates of the thermal resistance of the IWI wall obtained with the active method using the Bayesian inversion under uncertainty with

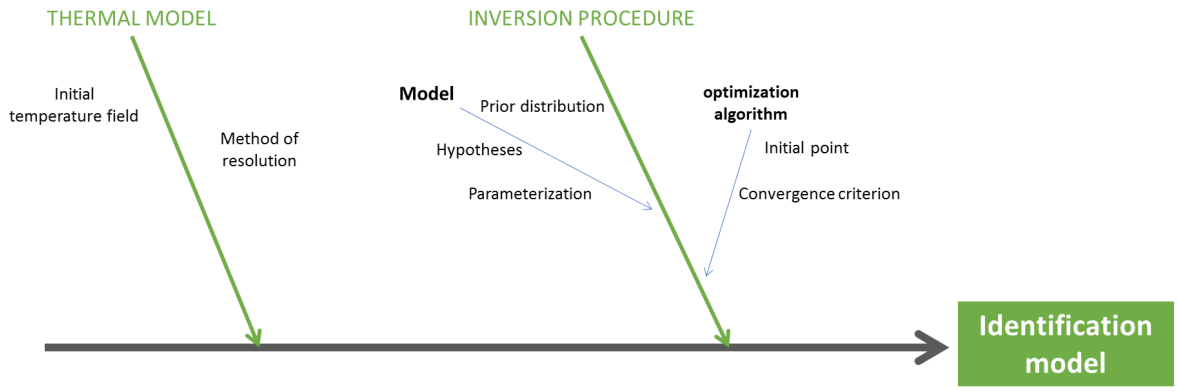

Figure 6. Ishikawa diagram for the identification model.

those obtained with the steady-state guarded hot box at CSTB, France in comparable experimental conditions ($T = 10\,°\text{C}$ and $\Delta T = 20\,°\text{C}$). As discussed section 3.3, many calibration parameters are not identifiable but the thermal conductivity of the insulation material k_2 should be identifiable. The comparison of the posterior distribution of k_2 with the experimental result obtained by LNE using the guarded hot plate method is also used as an indication of the performance of the Bayesian inversion method. Indeed, the thermal resistance of the insulation layer (calculated as $R_2 = l_2/k_2$) is far the most important contribution to the global thermal resistance of the IWI wall. A sensitivity study is performed to show the effect of duration and input uncertainties on the results of the Bayesian inversion.

3.5.1. Guarded hot plate results The guarded hot plate apparatus [ISO 8302:1991, 1991] determines steady-state thermal transmission properties of flat slab specimens having a low thermal conductivity. It uses the one-dimensional steady-state thermal conductivity equation. The relative standard uncertainty associated with GHP results is evaluated around 0.5%.

To conduct the measurement, we have cut two specimen of 600×600 mm from IWI coming from the same batch than those used to build the test wall. The measurements in the guarded hot plate were done at $T = 10\,°\text{C}$ mean temperature and $\Delta T = 15\,°\text{C}$. The result is computed as a mean over 8 hours after the steady state is reached. Results are displayed in Table 1. Tabulated values for the plasterboard and the cinderblock are given in Table 2.

3.5.2. Guarded hot box results The guarded hot box [ISO 8990:1994, 1994] assesses the thermal performance of walls at full scale. The wall to be tested is positioned between two ambient conditions: one hot and one cold. Here, the complete wall 2×2 m was measured in a GHB at CSTB, France at $T = 10\,°\text{C}$ and $\Delta T = 20\,°\text{C}$. The result is computed as a mean over 10 hours after the steady state is reached. Under these conditions, the thermal resistance of the specimen wall using the GHB is given by the

Layer	Heat capacity of unit area cw /J m^{-3} K	Thermal conductivity k /W m^{-1} K^{-1}	Thermal resistance R /m^2 K W^{-1}
EPS	$cw_2 = 1.35 \times 10^4$	$k_2 = 0.031$	$R_2 = 3.85$
EPS + Plasterboard	-	-	3.9

Table 1. Measured thermal performance on GHP.

Layer	Heat capacity of unit area cw /J m^{-3} K	Thermal conductivity k /W m^{-1} K^{-1}	Thermal resistance R /m^2 K W^{-1}
Plasterboard	$cw_1 = 7.30 \times 10^4$	$k_1 = 0.250$	0.05
Cinderblock	$cw_3 = 9.25 \times 10^4$	$k_3 = 0.850$	0.2

Table 2. Tabulated thermal performance values.

95% coverage interval defined by 4.08 ± 0.86 m^2 K W^{-1}, see details in Appendix A.

3.5.3. Active method coupled with Bayesian inversion Measurements recorded every two seconds for 24 hours are displayed in Figure 7 for the surface temperatures $y = Tsi$ and Tse and in Figure 8 for the absorbed flux q_{int} ($X = (Tse, q_{int})$). It can be observed that the absorbed flux becomes constant after 10 hours. For computational issues, measurements are sampled every 300 seconds for a total of $N = 289$ measurements.

A sensitivity analysis is performed to show the effects of duration and experimental uncertainties on the estimation of both the thermal conductivity k_2 of the insulation layer (EPS) and the estimation of the global thermal resistance R.

Table 3 describes the three uncertainty configurations ("no input uncertainty", "low level", "medium level") considered in the study. It is important to note that $u(Tsi) = u(Tse)$ in all configurations due to the experimental setting. The case "no input uncertainty" corresponds to the classical modelling where the input uncertainty is not taken into account but the output uncertainty is set to its experimental value $u(Tsi) = 0.5\,°C$. The case "low level input uncertainty" corresponds to the case where all experimental uncertainties would have been underestimated. The case "medium level uncertainty" corresponds to taking into account all the experimental values of uncertainties provided by LNE. This configuration is recommended *a priori*.

The effect of duration is studied for the recommended "medium level of uncertainty" and the effect of uncertainty is studied for the duration 24 hours. The resulting labels used in the legends of Figures 9, 10 and 11, are displayed in Table 4.

To conduct the Bayesian analysis, uniform prior distributions are assigned to the calibration parameters, whose bounds are displayed in Table 5. The resulting prior for the thermal resistance is obtained with Monte Carlo simulations from (12) and displayed as the grey histogram in Figure 10. The prior distribution for the excess

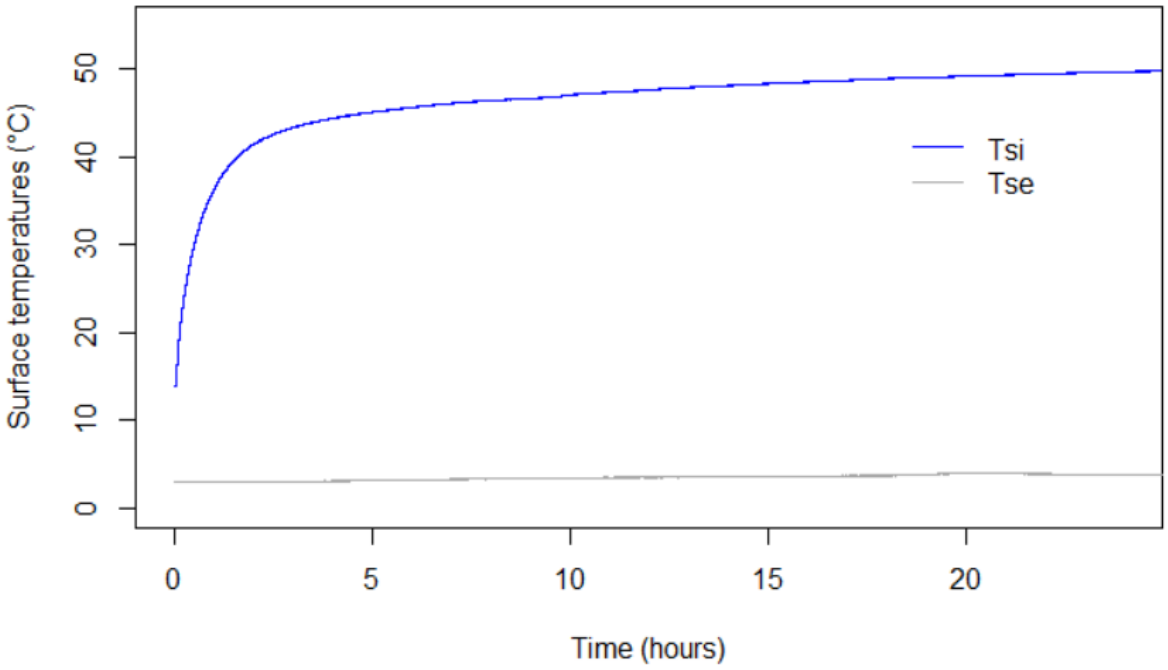

Figure 7. Surface temperature measurements for the IWI wall placed in the energy room REBECCA at LNE, France.

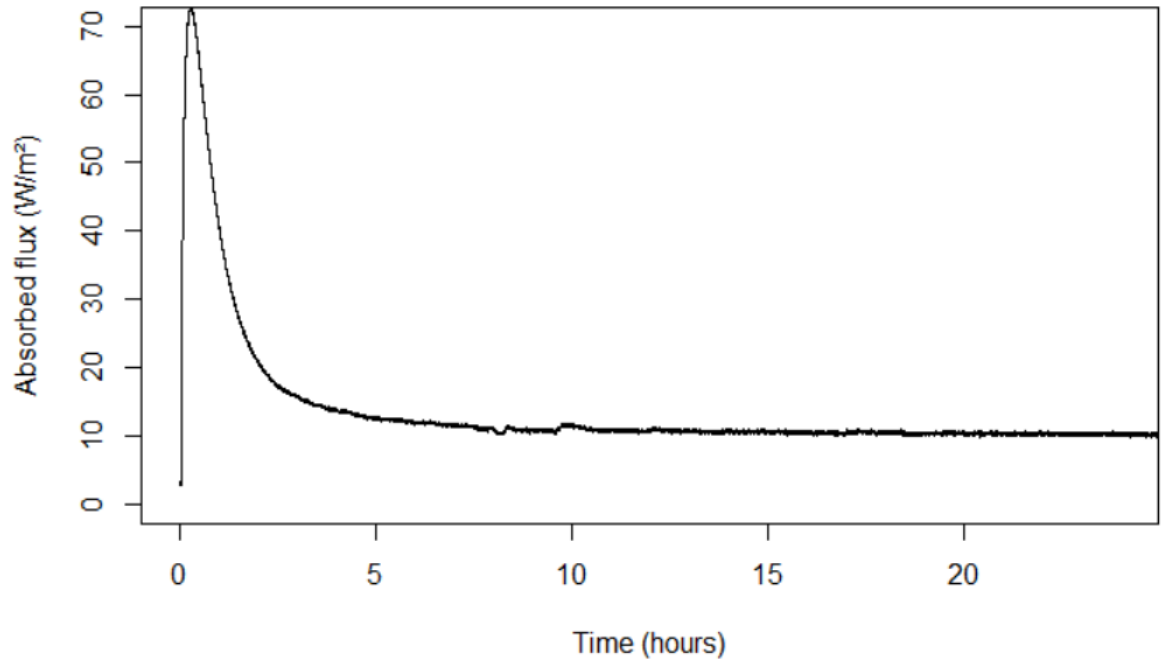

Figure 8. Absorbed flux measurements for the IWI wall placed in the energy room REBECCA at LNE, France.

variance parameter is chosen as $\pi(\sigma^2) \sim \text{InvChi}^2(\nu_0, s_0^2)$ with $\nu_0 = 2$ and $s_0^2 = 0$ to make it poorly informative as explained in section 2.2. Prior distributions of uncertain inputs in the vector $X = (Tse^T, q_{int}^T)^T$ are modeled following (4) with

$$\Sigma_\zeta = \begin{pmatrix} \Sigma_{Tse} & 0 \\ 0 & \Sigma_{q_{int}} \end{pmatrix} \tag{13}$$

where $\Sigma_{Tse} = \text{diag}(\{u^2(Tse)\}_N)$ and $\Sigma_{q_{int}} = \text{diag}(\{u^2(q_{int})\}_N)$ are the diagonal matrices of dimension $N \times N$ of reported variances of Tse and q_{int} respectively. Similarly, the covariance matrix of output observations y is chosen diagonal as $\Sigma_\epsilon = \text{diag}(\{u^2(Tsi)\}_N)$.

The MCMC procedure described in Algorithm 1 was run for each case from Table 4 with 50000 iterations, a burn-in of 20000 iterations and a thinning of 30 iterations. For each case, we controlled that the acceptance rate falls between 15% and 30%. For the "no input uncertainty" case the number of parameters is 8 (number of calibration parameters), whereas in the two other cases the propagation of input uncertainties involves $2N$ additional parameters corresponding to the elements of vector X, for a total of 586 parameters.

Level of uncertainty	$u(Tsi)$ /°C	$u(Tse)$ /°C	$u(q_{int})$ /W m^{-2}
no input uncertainty	0.5	-	-
low level	0.1	0.1	$1\%q_{int}$
medium level	0.5	0.5	$3\%q_{int}$

Table 3. Description of uncertainty configurations.

	Duration	
Level of uncertainty	12h	24h
no input uncertainty	-	24h_no_uncertainty
low level	-	24h_T001_Q1pct
medium level	12h_T005_Q3pct	24h_T005_Q3pct

Table 4. Labels used in the legends of plots resulting from the choice of duration and uncertainty configurations.

Results for the thermal conductivity of the insulation layer (EPS, Expanded Polystyrene) Figure 9 shows the effect of duration on the estimation of the thermal conductivity k_2 for the medium uncertainty level. The comparison with the guarded hot plate result (GHP, see section 3.5.1) displayed as the black dashed Gaussian distribution shows that the posterior estimate of k_2 is biased for 12 hours whereas the posterior estimate for 24

Layer	Thickness /m	Thermal conductivity k /W m^{-1} K^{-1}	Heat capacity of unit area cw /J m^{-2} K^{-1}
Plasterboard	$l_1 = 0.013$	$0.2 \leq k_1 \leq 0.4$	$7 \times 10^5 \leq cw_1 \leq 8 \times 10^5$
EPS	$l_2 = 0.120$	$0.02 \leq k_2 \leq 0.04$	$1 \times 10^4 \leq cw_2 \leq 3 \times 10^4$
Cinderblock	$l_3 = 0.150$	$0.7 \leq k_3 \leq 1.2$	$8.5 \times 10^5 \leq cw_3 \leq 2 \times 10^6$
Exterior coating	$l_4 = 0.015$	$0.5 \leq k_4 \leq 1.2$	$1 \times 10^6 \leq cw_4 \leq 2 \times 10^6$

Table 5. Caracterisation of each layer: thickness (assumed known in this application) and bounds for the uniform prior distributions of the thermal parameters, found in the literature.

hours is unbiased (the posterior distribution of k_2 is centered on the GHP best estimate). In other words, for 24 hours, the estimate of the thermal conductivity of the insulation material (k_2) is consistent with the physical value assessed with the guarded hot plate method.

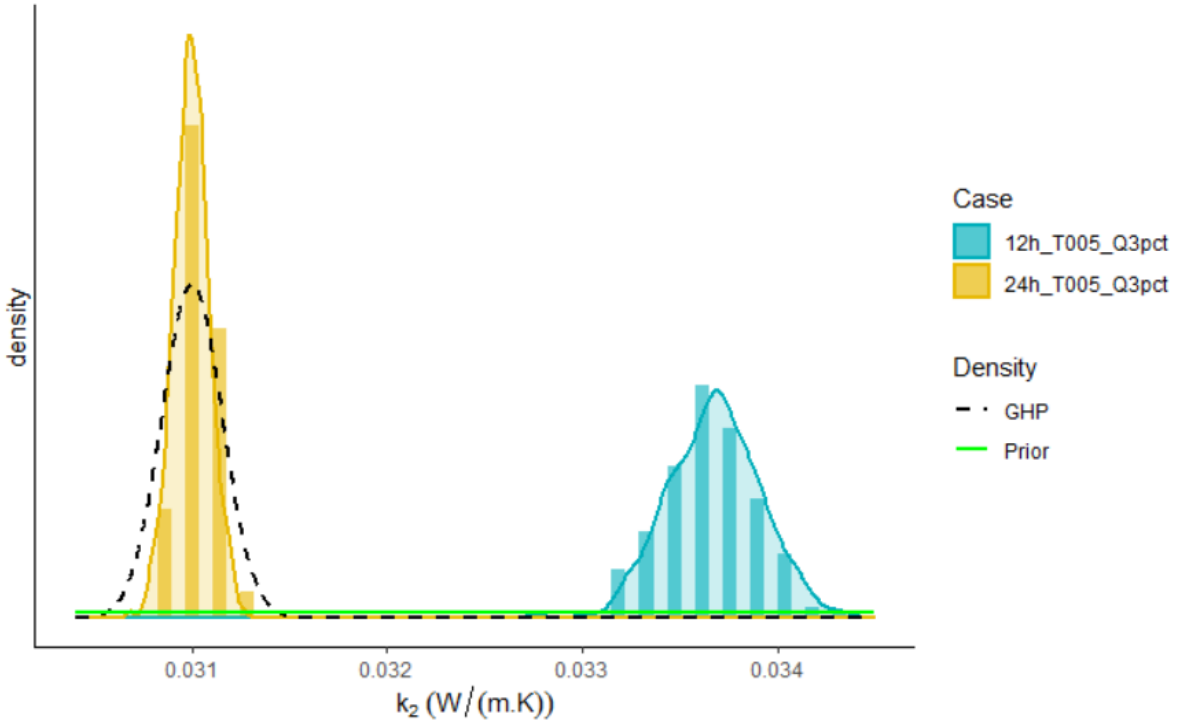

Figure 9. Histograms of the posterior samples for k_2 obtained after 12 hours and 24 hours and plots of the Gaussian distribution associated with the guarded hot plate (GHP) result and the prior distribution.

Table 6 gives the posterior estimates for all the uncertainty configurations. It can be observed that for 24 hours, all posterior results are consistent with the GHP result (the best estimate of the GHP 0.031 is included in the 95% Bayesian credible intervals).

It is important to note that the number of significant digits provided on the GHP result does not allow to compare the posterior results in terms of bias because all rounded posterior mean results are unbiased equal to 0.031. So the comparison with the GHP result does not allow to study the effect of uncertainty but globally says that the Bayesian methodology provides unbiased estimates of k_2 (w.r.t GHP result) and then of R_2 for a 24 h observation.

Duration /h	$u(Tsi)$ /°C	$u(Tse)$ /°C	$u(q_{int})$ /W m^{-2}	$\hat{k}_2$ /W m^{-1} K^{-1}	$u(\hat{k}_2)$ /W m^{-1} K^{-1}	Shortest 95% CI /W m^{-1} K^{-1}
24	0.1	-	-	0.0309	0.0001	$[0.0307, 0.0311]$
24	0.5	-	-	0.0309	0.0001	$[0.0307, 0.0311]$
24	0.1	0.1	$1\%q_{int}$	0.0309	< 0.0001	$[0.0307, 0.0310]$
12	0.5	0.5	$3\%q_{int}$	0.0337	0.0003	$[0.0333, 0.0342]$
24	0.5	0.5	$3\%q_{int}$	0.0310	< 0.0001	$[0.0308, 0.0312]$

Table 6. Results of the sensitivity study for the thermal conductivity k_2.

Results for the thermal resistance of the wall Figure 10 displays the results for the *global resistance of the wall* obtained with the guarded hot box method (GHB, see section 3.5.2) represented by a Gaussian approximation with 95% coverage interval (dashed vertical bars), the estimate of R_2 from the GHP result (see Table 1) and its 95% coverage interval (in black) and the posterior estimates of the thermal resistance and their associated 95% credible intervals (represented with horizontal turquoise and yellow dashes) obtained with the active method for the medium level of uncertainty for 12 hours and 24 hours respectively. Note that the histogram plot of the prior distribution shows that the prior for the global thermal resistance of the wall is consistent with the GHB result.

The 95% coverage interval for the GHB result covers all results (even those incomplete for only 12 hours) which means that the comparison which the GHB result cannot be used alone to evaluate the performance of the Bayesian method in the various configurations. We can underline that active solicitation coupled with Bayesian technique, which was developed for in-situ application, can lead to identification results as accurate as those obtained in GHP.

The ability of the Bayesian method to provide an unbiased estimate of R_2 was demontrated previously. Since R_2 represents 95% of the expected global thermal resistance R, the fact that the posterior estimate of the global resistance for 24 hours is closed to the best estimate of the GHB makes highly credible the ability of the Bayesian method to also provide an unbiased estimate of R for 24 hours.

The comparison with the *thermal resistance of the EPS* R_2 obtained from the GHP estimate of k_2 (black line) also shows that the estimate of the thermal resistance obtained after 12 hours (blue line) nearly allows to retrieve the thermal resistance of the EPS.

It is important to note that the comparison with the GHB result does not allow to study finely the effect of uncertainty in terms of resulting bias on the global thermal resistance.

Results of the sensitivity study in terms of the global thermal resistance are displayed in Table 7. We observe that the posterior uncertainty is similar (with two significant digits) for the configurations involving 24 hours records.

Finally, the plot of the posterior distribution of the thermal resistance of the wall for 24 hours and medium input uncertainty is displayed in Figure 11 with its 95% credible interval.

3.5.4. Remarks For both experiments conducted in a climatic chamber with similar controlled environmental conditions, the active method developed in the RESBATI project allows to estimate the thermal resistance with a relative uncertainty of less than 2% instead of 10% for the guarded hot box.

More generally, for in-situ measurements, the use of an active method should lessen the influence of uncontrolled environmental conditions so that, in practice, the same modelling should be used for in-situ measurements than for measurements obtained in the climatic chamber. Precisely, a sharp modelling is not required for the complex input quantities like weather, occupation,...

Duration /h	$u(Tsi)$ /°C	$u(Tse)$ /°C	$u(q_{int})$ /W m^{-2}	$\hat{R}$ /m^2 K W^{-1}	$u(\hat{R})$ /m^2 K W^{-1}	Shortest 95% CI /m^2 K W^{-1}
24	0.1	-	-	4.064	0.014	$[4.039, 4.091]$
24	0.5	-	-	4.072	0.014	$[4.045, 4.101]$
24	0.1	0.1	$1\%q_{int}$	4.083	0.014	$[4.054, 4.107]$
12	0.5	0.5	$3\%q_{int}$	3.759	0.025	$[3.712, 3.808]$
24	0.5	0.5	$3\%q_{int}$	4.058	0.014	$[4.031, 4.087]$

Table 7. Results of the sensitivity study for the global thermal resistance.

4. Conclusion and discussion

This paper presents a Bayesian approach for the indirect measurement of thermal parameters of a wall from thermal measurements obtained with thermocouples and fluxmeters using an active method. This work is part of the ANR RESBATI project whose main objective is to develop a portable measurement device for evaluating the thermal resistance of opaque building walls on site. The case study chosen in this paper concerns the analysis of measurements performed on an internal wall insulation (IWI) built within the project. The work takes advantage of the experimental work performed on the wall for its global thermal caracterisation in a guarded hot box and for the

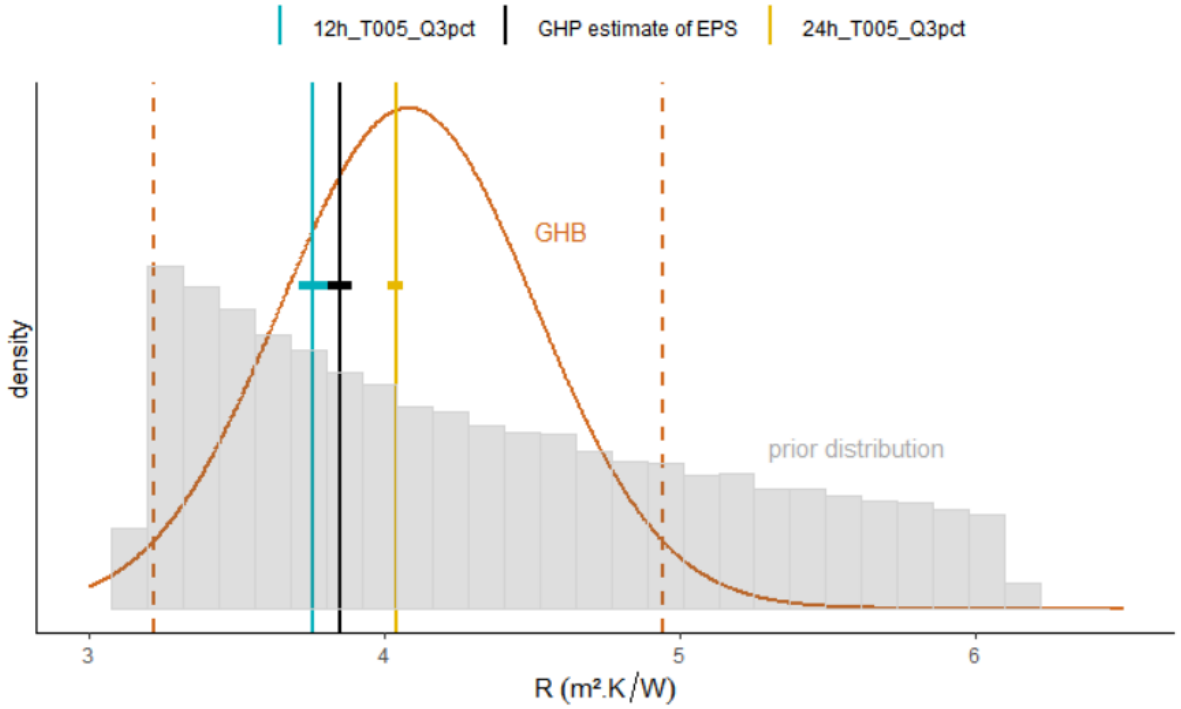

Figure 10. In grey: prior distribution of R, in chocolate: Gaussian distribution associated with the GHB estimate of R and its 95% coverage interval, in black: GHP estimate of R_2 and its 95% coverage interval, in turquoise: Bayesian estimate of R after 12 h with the medium uncertainty level and its 95% credible interval, in yellow: Bayesian estimate of R after 24 h with the medium uncertainty level and its 95% credible interval.

thermal caracterisation of the insulation layer performed with a guarded hot plate, for assessing the performance of the Bayesian uncertainty analysis.

The fully Bayesian approach is particularly suited for uncertainty quantification, especially when prior knowledge is available, and is used here for its ability to propagate input uncertainties in an inversion problem, which is in practice an issue rarely addressed with no consensus methodology so far up to our knowledge. The advocated uncertainty propagation approach is easy to apply since it consists in treating all uncertain inputs as calibration parameters and thus requires only a small adaptation of existing MCMC algorithms, for a slightly higher computational cost. For instance, in the case study, we experienced that the computational cost comes primarily from the duration.

Under the experimental conditions of the climatic chamber equipped with calibrated thermocouples and fluxmeters, this study demonstrates the efficiency of the Bayesian analysis of the measurements obtained with an active method to produce unbiased (w.r.t the guarded hot plate method) estimates of the thermal conductivity of the insulation layer (EPS) for 24 hours with a low associated standard uncertainty (less than 2%). Nevertheless, smaller observation time, e.g. 12h, has lead to a biased identification.

In this application, it appears that the impact of uncertainties is quite small and cannot be interpreted in terms of resulting bias w.r.t. a reference value. In particular,

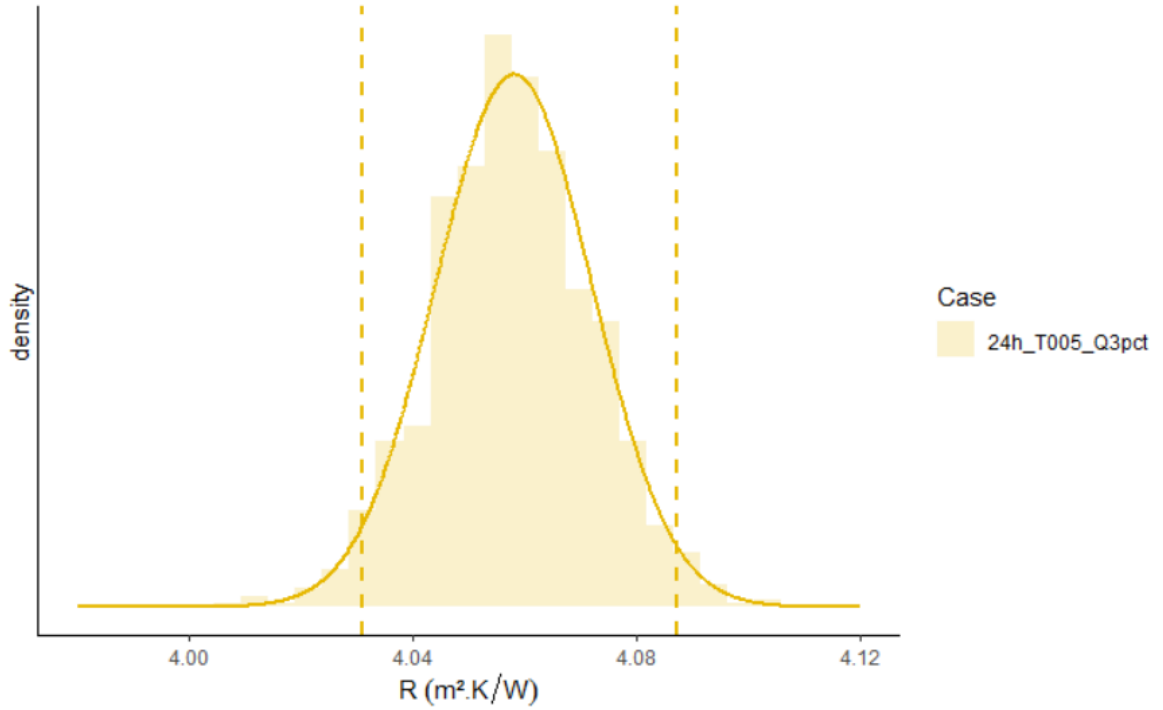

Figure 11. Plot of the posterior distribution of the global thermal resistance of the IWI wall obtained with the active method, and its associated 95% credible interval for 24 hours observations (vertical dashed lines).

due to the experimental settings we were not able to quantify the impact of input uncertainties on the estimated thermal parameters.

For setting input uncertainties, we recommend to perform calibrations and/or verifications of measurement means. If no input uncertainties are available, this study confirms the recommendation from the literature to set a small uncertainty on input parameters to help reducing bias.

The general formulation of the methodology makes it easily applicable to other types of walls and insulation. In this respect, one of the perspectives of the RESBATI project is to address sustainable materials like bio-sourced materials and raw earth considering a hygro-thermal model.

Acknowledgements

This research was made possible by support from ANR (Agence Nationale de la Recherche) the French National Research Agency through the project RESBATI under Grant agreement NANR-16-CE22-0010-02.

References

[ASHRAE, 2017] ASHRAE (2017). *ASHRAE handbook: Fundamentals : SI edition*. American Society of Heating, Refrigerating and Air-Conditioning Engineers, Atlanta, GA.

[Berger et al., 2016] Berger, J., Orlande, H. R., Mendes, N., and Guernouti, S. (2016). Bayesian inference for estimating thermal properties of a historic building wall. *Building and Environment*, 106:327 – 339.

[BIPM et al., 2008a] BIPM, IEC, IFCC, ILAC, ISO, IUPAC, IUPAP, and OIML (2008a). *Guide to the Expression of Uncertainty in Measurement, JCGM 100:2008, GUM 1995 with minor corrections*. BIPM.

[BIPM et al., 2008b] BIPM, IEC, IFCC, ILAC, ISO, IUPAC, IUPAP, and OIML (2008b). *Supplement 1 to the 'Guide to the Expression of Uncertainty in Measurement' – Propagation of distributions using a Monte Carlo method, JCGM 101:2008*. BIPM.

[Bodnar and Elster, 2014] Bodnar, O. and Elster, C. (2014). On the adjustment of inconsistent data using the birge ratio. *Metrologia*, 51:516.

[Bodnar et al., 2017] Bodnar, O., Link, A., Arendack, B., Possolo, A., and Elster, C. (2017). Bayesian estimation in random effects meta-analysis using a non-informative prior. *Statistics in Medicine*, 36(2):378–399.

[Box and Tiao, 1992] Box, G. and Tiao, G. (1992). *Bayesian Inference in Statistical Analysis*. Wiley.

[Chib and Greenberg, 1995] Chib, S. and Greenberg, E. (1995). Understanding the metropolis-hastings algorithm. *The American Statistician*, 49(4):327–335.

[Demeyer et al., 2021] Demeyer, S., Fischer, N., and Elster, C. (2021). Guidance on Bayesian uncertainty evaluation for a class of GUM measurement models. *Metrologia*, 58:1–13.

[François et al., 2020] François, A., Ibos, L., Feuillet, V., and Meulemans, J. (2020). Estimation of the thermal resistance of a building wall with inverse techniques based on rapid active in situ measurements and white-box or ARX blackbox models. *Energy & Buildings*, 226.

[Gelman et al., 2013] Gelman, A., Carlin, J. B., Stern, H. S., Dunson, D. B., Vehtari, A., and Rubin, D. B. (2013). *Bayesian Data Analysis, 3rd edition*. Chapman and Hall/CRC.

[Goffart et al., 2017] Goffart, J., Mara, T., and Wurtz, E. (2017). Generation of stochastic weather data for uncertainty and sensitivity analysis of a low-energy building. *Journal of Building Physics*, 41(1):41–57.

[Gori and Elwell, 2018] Gori, V. and Elwell, C. A. (2018). Estimation of thermophysical properties from in-situ measurements in all seasons: Quantifying and reducing errors using dynamic grey-box methods. *Energy & Buildings*, 167:290 – 300.

[Ha et al., 2020] Ha, T.-T., Feuillet, V., Waeytens, J., Zibouche, K., Thebault, S., Bouchie, R., Le Sant, V., and Ibos, L. (2020). Benchmark of identification methods for the estimation of building wall thermal resistance using active method: Numerical study for iwi and single-wall structures. *Energy and Buildings*, 224:110130.

[Heo et al., 2012] Heo, Y., Choudhary, R., and Augenbroe, G. (2012). Calibration of building energy models for retrofit analysis under uncertainty. *Energy and Buildings*, 47:550 – 560.

[Higdon et al., 2004] Higdon, D., Kennedy, M., Cavendish, J., Cafeo, J., and Ryne, R. (2004). Combining field data and computer simulations for calibration and prediction. *SIAM Journal on Scientific Computing*, 26(2):448–466.

[Iglesias et al., 2018] Iglesias, M., Sawlan, Z., Scavino, M., Tempone, R., and Wood, C. (2018). Bayesian inferences of the thermal properties of a wall using temperature and heat flux measurements. *International Journal of Heat and Mass Transfer*, 116:417 – 431.

[ISO 8302:1991, 1991] ISO 8302:1991 (1991). *Thermal Insulation Determination of Steady-State Thermal Resistance and Related Properties Guarded hot plate apparatus*. International Organization for Standardization.

[ISO 8990:1994, 1994] ISO 8990:1994 (1994). *Thermal insulation - Determination of steady-state thermal transmission properties - Calibrated and guarded hot box*. International Organization

for Standardization.

[Kaipio and Fox, 2011] Kaipio, J. P. and Fox, C. (2011). The bayesian framework for inverse problems in heat transfer. *Heat Transfer Engineering*, 32(9):718–753.

[Kennedy and O'Hagan, 2001] Kennedy, M. and O'Hagan, A. (2001). Bayesian calibration of computer models. *J. R. Statist. Soc. B*, 63(3):425–464.

[Klauenberg and Elster, 2016] Klauenberg, K. and Elster, C. (2016). Markov chain Monte Carlo methods: an introductory example. *Metrologia*, 53(1):S32.

[Koenen et al., 2019] Koenen, A., Marquis, D., Garcia, Y., Le Sant, V., Demeyer, S., Monchau, J.-P., Feuillet, V., Ibos, L., Ha, T., Gavérina, L., Dumoulin, J., Manceau, J.-L., Bouchié, R., Zibouche, K., and Lahlou, F. (2019). Evaluation of a research prototype for measuring and controlling the thermal resistance of building walls in active mode. *ITCC-ITES Conference*.

[Macdonald, 2002] Macdonald, I. A. (2002). *Quantifying the effects of uncertainty in building simulation*. University of Strathclyde. PhD thesis.

[Mana et al., 2012] Mana, G., Massa, E., and Predescu, M. (2012). Model selection in the average of inconsistent data: an analysis of the measured Planck-constant values. *Metrologia*, 49:492500.

[Metropolis et al., 1953] Metropolis, N., Rosenbluth, A. W., Rosenbluth, M. N., Teller, A. H., and Teller, E. (1953). Equation of state calculations by fast computing machines. *The Journal of Chemical Physics*, 21(6):1087–1092.

[NF EN ISO 10211:2017, 2017] NF EN ISO 10211:2017 (2017). *Thermal bridges in building construction Heat flows and surface temperatures Detailed calculations*. International Organization for Standardization.

[NF EN ISO 12567-1:2013, 2013] NF EN ISO 12567-1:2013 (2013). *Thermal performance of windows and doors Determination of thermal transmittance by the hot-box method Part 1: Complete windows and doors*. International Organization for Standardization.

[Perrin and Durantin, 2019] Perrin, G. and Durantin, C. (2019). Taking into account input uncertainties in the bayesian calibration of time-consuming simulators. *Journal de la Société Française de Statistique*, 160:24 – 46.

[Rasmussen and Williams, 2006] Rasmussen, C. E. and Williams, C. K. I. (2006). *Gaussian Processes for Machine Learning*. MIT Press.

[Robert and Casella, 2013] Robert, C. and Casella, G. (2013). *Monte Carlo statistical methods*. Springer Science & Business Media.

[Rodler et al., 2019] Rodler, A., Guernouti, S., and Musy, M. (2019). Bayesian inference method for in situ thermal conductivity and heat capacity identification: Comparison to iso standard. *Construction and Building Materials*, 196:574 – 593.

[Rouchier, 2018] Rouchier, S. (2018). Solving inverse problems in building physics: An overview of guidelines for a careful and optimal use of data. *Energy & Buildings*, 166:178 – 195.

[Saltelli et al., 2004] Saltelli, A., Tarantola, S., Campolongo, F., and Ratto, M. (2004). *Sensitivity Analysis in Practice: A Guide to Assessing Scientific Models*. Wiley.

[Santner and Notz, 2003] Santner, T. J. and Notz, W. (2003). *The design and analysis of computer experiments*. Springer Verlag, Springer Series in Statistics.

[Simon et al., 2018] Simon, L. D., Iglesias, M., Jones, B., and Wood, C. (2018). Quantifying uncertainty in thermophysical properties of walls by means of bayesian inversion. *Energy and Buildings*, 177:220 – 245.

[Thébault and Bouchié, 2018] Thébault, S. and Bouchié, R. (2018). Refinement of the isabele method regarding uncertainty quantification and thermal dynamics modelling. *Energy and Buildings*, 178:182 – 205.

[Toman and Possolo, 2009] Toman, B. and Possolo, A. (2009). Laboratory effects models for interlaboratory comparisons. *Accreditation and Quality Assurance*, 14:553–563.

[Wang and Zabaras, 2004] Wang, J. and Zabaras, N. (2004). Hierarchical bayesian models for inverse problems in heat conduction. *Inverse Problems*, 21(1):183–206.

[XP ISO/TS 28037:2013, 2013] XP ISO/TS 28037:2013 (2013). *Détermination et utilisation des*

fonctions d'étalonnage linéaire. International Organization for Standardization.

Appendix A. Details on GHB uncertainty evaluation at CSTB, France

The estimated U value for the IWI wall for a mean temperature T =10 °C is

$$U = 0.245\,\mathrm{W\,m^{-2}\,K} \tag{A.1}$$

The global thermal resistance is

$$R = \frac{1}{U} \tag{A.2}$$

Denoting $u(U)$ the standard uncertainty associated with U, GUM [BIPM et al., 2008a] uncertainty propagation gives

$$u(R) = \frac{u(U)}{U^2} = 0.43\,\mathrm{m^2\,K\,W^{-1}} \tag{A.3}$$

Equivalently, the 95% coverage interval associated with R is

$$4.08 \pm 0.86\,\mathrm{m^2\,K\,W^{-1}} (k = 2) \tag{A.4}$$

The following describes the uncertainty evaluation of U. The specimen is installed on a surrounding wall, the measurement zone is larger than the sample surface so that, in steady state conditions, a part of the heating power injected in the measurement zone ϕ_{in} is split between :

- A thermal flow through the metering box, ϕ_{out}, controlled to be neglectable by controlling the guarded zone temperature equal to the measuring zone temperature. The residual thermal flow through the metering box is then controlled to be neglectable by measuring it using a thermopile ($\phi_{out} = 0\,\mathrm{W}$);
- A thermal flow through the specimen ϕ_{sp};
- A thermal flow through the surrounding wall ϕ_{sur};
- A thermal flow through thermal bridge between the sample and surrounding wall ϕ_{edge};

The thermal flow through the specimen is then obtained by

$$\phi_{sp} = \phi_{in} - \phi_{sur} - \phi_{edge} \tag{A.5}$$

The U value is then obtained by

$$U = \frac{\phi_{sp}}{A_{sp}\,(\theta_{n,i} - \theta_{n,e})} \tag{A.6}$$

where A_{sp} is the surface of the specimen, $\theta_{n,i}$ and $\theta_{n,e}$ are the environment internal/external temperatures included by air temperature $(\theta_{c,i}, \theta_{c,e})$ and radiant temperature viewed by the specimen $(\theta_{r,i}, \theta_{r,e})$ temperatures:

$$\theta_{n,i} = F_{c,i}\theta_{c,i} + (1 - F_{c,i})\,\theta_{r,i} \tag{A.7}$$

$$\theta_{n,e} = F_{c,e}\theta_{c,e} + (1 - F_{c,e})\,\theta_{r,e} \tag{A.8}$$

where $F_{c,i}$ and $F_{c,e}$ are convective fractions.

Radiant temperatures $(\theta_{r,i}, \theta_{r,e})$ are described in Annex A of NF EN ISO 12567-1 [NF EN ISO 12567-1:2013, 2013] as an explicit function of surface temperatures of the specimen $(\theta_{s,i}, \theta_{s,e})$ and the baffle $(\theta_{b,i}, \theta_{b,e})$ panel situated in front of each side.

The thermal flow through the surrounding wall ϕ_{sur} and convective fractions $F_{c,i}$ and $F_{c,e}$ are obtained using a calibration process as described in NF EN ISO 12567-1 [NF EN ISO 12567-1:2013, 2013]. This calibration consists in using homogeneous insulated calibration panels as specimen. The thermal resistance of these calibration panels have been measured using guarded hot plate method so that their R-values are well known. Measuring surface temperatures during the calibration test in the guarded hot box make possible determining both R_{sur} (and then ϕ_{sur}) as a function of average support wall temperature, and convective fractions as a function of thermal flow through the specimen, using linear regression techniques. The linear regression coefficients are then used to predict ϕ_{sur}, $F_{c,i}$ and $F_{c,e}$ during all experiment. The uncertainty on this prediction is estimated using less squares methods [XP ISO/TS 28037:2013, 2013].

The uncertainty on the thermal flow through thermal bridge between the sample and surrounding wall ϕ_{edge} is estimated by simulating each junction [NF EN ISO 10211:2017, 2017]. A sensibility analysis has been provided on each unknown input: thermal conductivity of wood element for instance may vary between 0.13 to 0.18 W/(m.K). The possible variation interval of the calculated psi-values, estimated with this sensibility analysis, is then used to define a uniform law with standard deviation:

$$u_{\psi_{edge}} = \frac{\psi_{edge_max} - \psi_{edge_min}}{\sqrt{3}} \tag{A.9}$$

Finally, all errors are propagated using GUM recommendations [BIPM et al., 2008a].

Appendix B. R code

The R code associated with the low and medium uncertainty levels implementing 1 is given in the Supplementary material.

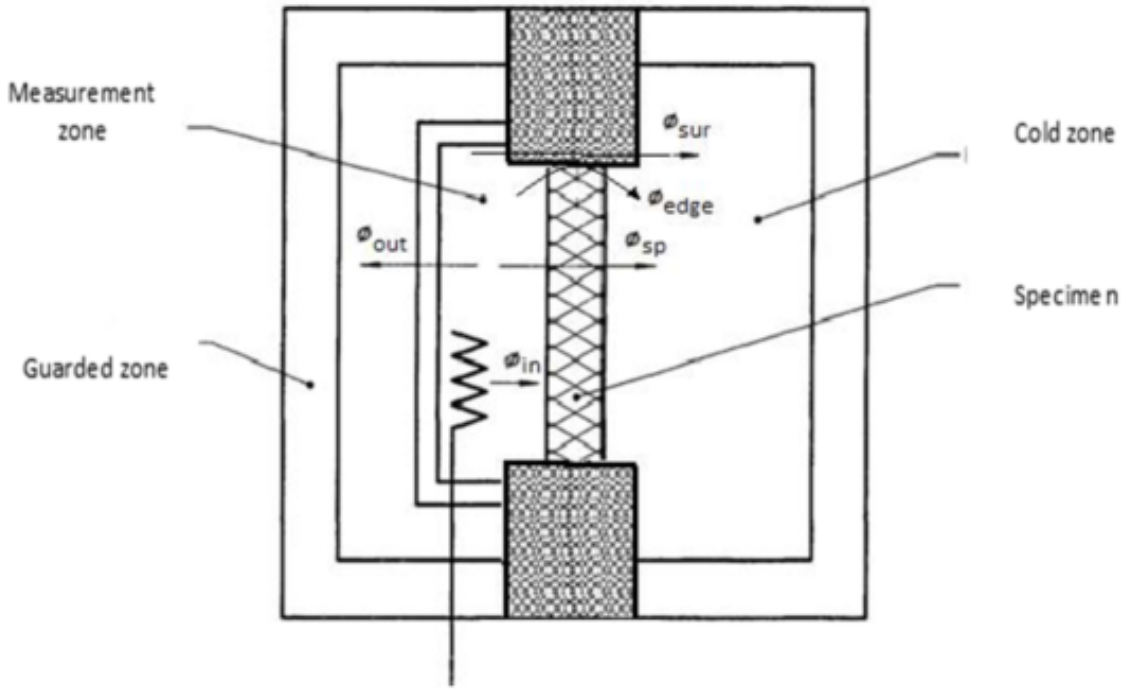

Figure A1. Notations for uncertainty propagation in GHB at CSTB, France.